

The viscous sublayer revisited—exploiting self-similarity to determine the wall position and friction velocity

P. Henrik Alfredsson · Ramis Örlü · Philipp Schlatter

Received: 27 October 2010/Revised: 20 January 2011/Accepted: 27 January 2011/Published online: 12 February 2011
© Springer-Verlag 2011

Abstract In experiments using hot wires near the wall, it is well known that wall interference effects between the hot wire and the wall give rise to errors, and mean velocity data from the viscous sublayer can usually not be used to determine the wall position, nor the friction velocity from the linear velocity distribution. Here, we introduce a new method that takes advantage of the similarity of the probability density distributions (PDF) or rather the cumulative distribution functions (CDF) in the near-wall region. By using the velocity data in the CDF in a novel way, it is possible to circumvent the problem associated with heat transfer to the wall and to accurately determine both the wall position and the friction velocity. Prior to its exploitation, the self-similarity of the distribution functions of the streamwise velocity fluctuations within the viscous sublayer is established, and it is shown that they can accurately be described by a lognormal distribution.

1 Introduction

Wall-bounded turbulent flows are usually divided into four regions: the viscous sublayer, the buffer region, the overlap or logarithmic layer, and the wake or core region. In this paper, we focus on the viscous sublayer, which extends to about 5 viscous units ($\ell_* = \nu/u_\tau$, where ν is the viscosity and u_τ the friction velocity) from the wall. The importance of the viscous sublayer for the understanding of wall-bounded turbulent flows cannot be overestimated since it determines the wall shear stress ($\tau_w = \rho u_\tau^2$, where ρ

denotes the density), which is a scaling parameter for both the mean velocity and the Reynolds stresses.

In an experiment, the physical size of the viscous sublayer is usually very thin, and it is hard to obtain accurate velocity measurements within this region. So, for instance, it is an accurate determination of the wall with respect to the measurement probe within one viscous unit, which for a free-stream velocity (U_∞) of 40 m/s is roughly $\ell_* = 10 \mu\text{m}$, not easily achieved through optical or mechanical measurements (see e.g. Örlü et al. 2010, for a review). Moreover, the friction velocity is a quantity that is hard to measure accurately, an exception being oil-film interferometry (Rüedi et al. 2009; Pailhas et al. 2009), which, however, is not a standard practice in most laboratories. One possibility is to utilize the linear mean velocity profile ($U^+ = y^+$, where U and y denote the mean streamwise velocity and wall-normal distance, respectively, and the superscript $+$ indicates normalizing with inner units, i.e. u_τ and ℓ_*) in order to determine both of the mentioned quantities (see for instance Durst et al. 1996). However, for hot-wire measurements, this is impeded by the fact that the measurements are affected by heat transfer to the wall. On the other hand, this effect can also advantageously be exploited to determine the wall position, since for a given hot wire, the measured voltage in quiescent air is dependent on the hot-wire probe, and its operating parameters as well as the distance to the wall. Consequently, a suitable calibration enables the determination of the wall position, as described and employed in Durst et al. (1987, 2001). Note, however, that this method is restricted to work only under no flow conditions.

There are many studies dealing with various correction schemes for hot-wire errors close to the wall (see e.g. Oka and Kostic 1972; Hebbbar 1980; Bhatia et al. 1982; Chew et al. 1995; Durst and Zanoun 2002; Wenzhong et al. 2006,

P. H. Alfredsson (✉) · R. Örlü · P. Schlatter
Linné FLOW Centre, KTH Mechanics,
100 44 Stockholm, Sweden
e-mail: phal@mech.kth.se

just to mention a few). However, in some sense, this is not such an interesting issue from a fundamental point of view, because the viscous sublayer by itself is fairly well known, especially when it comes to the mean velocity distribution, but also for various statistical quantities of the fluctuating components. However, what is interesting is, if and how data measured close to the wall that are affected by wall interference can be used to determine the wall position as well as the friction velocity. The present paper shows that this is indeed possible by exploiting the self-similarity of the cumulative distribution function (CDF) of the measured streamwise velocity in a novel way.

In the following, the experimental and numerical databases used throughout the paper are documented in Sect. 2. After describing the behavior of the streamwise velocity fluctuations throughout the viscous sublayer and establishing the self-similarity of the distribution functions in Sect. 3, the established self-similarity is exploited in Sect. 4 to determine the wall location and friction velocity. Section 5 concludes the present paper.

2 Databases

The results presented in the present paper are based on one experimental dataset pertaining to a zero pressure-gradient (ZPG) turbulent boundary layer (TBL) and two numerical databases for both plane channel and boundary-layer flow. In this section, we provide a brief summary of these datasets; detailed descriptions are provided in the original publications.

The experiments were performed in the MTL (Minimum Turbulence Level) wind tunnel at KTH Stockholm. Special care has been taken to ensure a constant pressure along the flat plate by adjusting the tunnel roof. Whereas the velocity signal has been recorded by hot-wire probes, the skin friction has been measured independently by oil-film interferometry. For the present paper, the measurements at a Reynolds numbers of $Re_\theta = 2,500$ are used, where Re_θ denotes the Reynolds number based on free stream velocity and momentum loss thickness. The full experimental setup is described in Örlü (2009) and Schlatter et al. (2009).

Both the boundary-layer and channel simulations were performed using a fully spectral method to solve the time-dependent, incompressible Navier–Stokes equations (Chevalier et al. 2007). In the wall-parallel directions, Fourier series with dealiasing are used whereas the wall-normal direction is discretized with Chebyshev polynomials. The resolution in the wall-parallel planes has been fixed in terms of wall units, i.e. $\Delta x^+ < 10$ and $\Delta z^+ < 5$. The simulations of channel flow at $Re_\tau = 590$, where Re_τ denotes

the friction Reynolds number or so-called Kármán number have been performed in a similar way as Moser et al. (1999) using a periodic box of size $2\pi h \times \pi h$ in the streamwise and spanwise directions, respectively, with h denoting the channel half-height. The data presented here are based on a total of 12 full velocity fields saved from this simulation.

The DNS of the spatially evolving turbulent boundary layer has been performed by employing a laminar inflow which is then perturbed leading to rapid laminar-turbulent transition and subsequently to fully developed turbulent flow, spanning the range of Reynolds number $Re_\theta \approx 500$ to $Re_\theta \approx 4,300$. This particular simulation is one of the largest turbulence simulations to date, using approximately 7.5×10^9 grid points. Thus, only time series at selected Reynolds numbers and wall-normal positions could be saved. Further details are given in Schlatter et al. (2009) and Schlatter and Örlü (2010).

3 Velocity fluctuations in the near-wall region

3.1 Near-wall y -dependence

The instantaneous streamwise velocity in the near-wall region of wall-bounded turbulent flows can be expanded as (see e.g. Monin and Yaglom 1971)

$$u(t) = a_1(t)y + a_2(t)y^2 + a_3(t)y^3 + a_4(t)y^4 + \dots$$

and by taking the time average ($\bar{\quad}$) we get

$$U = \overline{u(t)} = \bar{a}_1 y + \bar{a}_2 y^2 + \bar{a}_3 y^3 + \bar{a}_4 y^4 + \dots,$$

where

$$\bar{a}_1 = \frac{u_\tau^2}{\nu}, \quad \bar{a}_2 = \frac{1}{2\mu} \frac{d\bar{p}}{dx}, \quad \bar{a}_3 = 0, \quad \bar{a}_4 \neq 0.$$

For a zero pressure-gradient turbulent boundary layer, this amounts to

$$U^+ = y^+ + \bar{a}_4^+ y^{+4} + \dots,$$

where \bar{a}_4^+ can be obtained from DNS to give a value of about -2×10^{-4} (see e.g. Örlü et al. 2010). This indicates that the mean velocity profile only deviates from the linear profile with 5% at $y^+ = 6$. In the case of a fully developed turbulent channel flow, we can write the pressure-gradient term

$$\bar{a}_2^+ = -\frac{2}{h^+} = -\frac{2}{Re_\tau},$$

where h is the channel half-height. Only for very low Reynolds numbers (or equivalently small h^+) does this term become larger than the fourth-order term. In fact, for

channel flows, the quadratic term becomes negligible for $h^+ > 500$, so that the value of the quartic term in channel flows becomes similar to the one in ZPG TBL flows (Örlü et al. 2010).

One may also find the variance of the fluctuating velocity as

$$\text{var}(u) = \overline{(u - U)^2} = \overline{(a_1 - \bar{a}_1)^2} y^2 + 2\bar{a}_1 \bar{a}_2 y^3 + \dots$$

and if we normalize it with the local velocity (here we assume that $\bar{a}_2 = 0$) we obtain

$$\frac{\text{var}(u)}{U^2} = \frac{\overline{(a_1 - \bar{a}_1)^2}}{\bar{a}_1^2} + 2 \frac{\bar{a}_1 \bar{a}_2}{\bar{a}_1^2} y + \dots$$

This shows that the variance normalized with the local velocity is constant (with respect to y) close to the wall and indicates that the probability density distribution (PDF) is self-similar in the same region. In fact, the limiting behavior of the above quantity is directly related to the variance of the fluctuating wall shear stress (Alfredsson et al. 1988)

$$\frac{\text{var}(\tau)}{\bar{\tau}^2} = \lim_{y \rightarrow 0} \frac{\text{var}(u)}{U^2}$$

Classical inner scaling for the Reynolds normal stresses within the inner region of channel and ZPG TBL flows, indicates that there is a weak Reynolds number dependence in the limiting value of the higher-order moments (Buschmann et al. 2009; Schlatter and Örlü 2010).¹ This stems primarily from scales of the order of the outer length scales, which hints at the persistence of Reynolds number effects in even high Reynolds number flows (Buschmann and Gad-el-Hak 2010).

3.2 Distribution functions of the streamwise velocity

To start with, it is interesting to point out that the scaling of the streamwise velocity within the viscous sublayer has usually only been considered in terms of its time-averaged quantities (Khoo et al. 1997; Buschmann et al. 2009). It has been noted in earlier studies (see e.g. Eckelmann 1974; Alfredsson et al. 1988) that the streamwise velocity fluctuations are very similar (in fact, highly correlated to the velocity gradient at the wall when taking the structure inclination angle into account, as shown by Marusic and Heuer 2007) throughout the viscous sublayer, which indicates that there exists a self-similarity of the PDFs of the streamwise velocity fluctuations in the viscous sublayer.

¹ The situation for pipe flows is, due to the lack of both resolved experimental and numerical data spanning a sufficient Reynolds number range, unclear (Hultmark et al. 2010), although the recent pipe flow DNS by Wu and Moin (2009) indicates an increase in the limiting values with increasing Reynolds number.

Earlier studies regarding the self-similarity of the PDFs in wall-bounded turbulence have mainly focussed on the overlap region (Tsuji and Nakamura 1999; Lindgren et al. 2004; Morrison et al. 2004).

Here, however, we intend to consider the distribution functions itself within the viscous sublayer as depicted in Fig. 1, where direct numerical simulation (DNS) data from a zero pressure-gradient turbulent boundary layer at $Re_\theta \approx 2,500$ (Schlatter and Örlü 2010) are presented. The figure shows contours of the probability density, together with the mean velocity, the maximum of the PDF as well as the highest and lowest velocities as function of y^+ . Subplot (Fig. 1a) is plotted in the standard way with u^+ against $\log y^+$. The graph shows the expected behavior, i.e. the widest PDF is found in the buffer region, and the PDFs are asymmetric on both sides of $y^+ \approx 13$. Close to the wall, $y^+ < 13$, velocities that are lower than the local mean value occur most often. At distances $y^+ > 13$, the opposite is the case as already shown by Eckelmann (1974).

Focussing on the near-wall region, Fig. 1b, the same data are now plotted as $\log u^+$ against $\log y^+$. As can be seen, the contour lines of the PDF become almost parallel from the wall up to about $y^+ = 10$ (at least for the low-velocity part) in this plot. This indicates that the PDFs are nearly self-similar in this region, as will be discussed in the following. This can in particular be evinced from Fig. 2, where DNS data from a channel flow at $h^+ = 590$ with a finer resolution within the viscous sublayer have been employed.

As a side note, it is interesting to point out that the DNS observes rare incidents of backflow, of the order of 0.01% of the time at a given position within the viscous sublayer, which explains the break off of the lines indicating the lowest occurring velocity fluctuations. For a discussion of this phenomenon, see Örlü and Schlatter (2011), where its omnipresence throughout the viscous sublayer for zero and favorable pressure-gradient flows with different simulation methods is established.

3.3 The cumulative density distribution

In the present study, we utilize the CDF of the streamwise velocity, rather than the PDF, in a way so that the influence of the heat transfer from a hot wire to the wall can be handled in such a way that accurate estimates of the wall position and the friction velocity can be obtained. The CDF (F) is related to the PDF (f) through the following relation

$$F(u) = \int_{-\infty}^u f(s) ds, \text{ where } 0 \leq F(u) \leq 1 \text{ and} \tag{1}$$

$$F(u) \rightarrow 1 \text{ as } u \rightarrow +\infty. \tag{2}$$

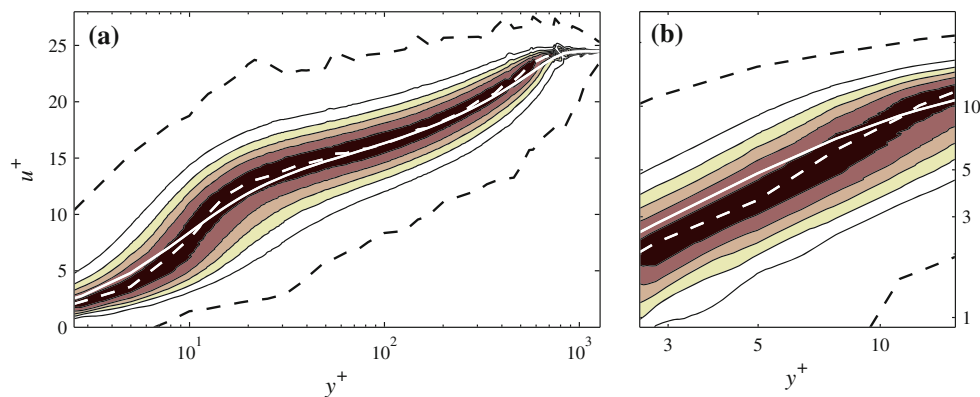


Fig. 1 Mean streamwise velocity over wall-normal position scaled in inner variables, U^+ versus y^+ , (white line) plotted above the PDF of the instantaneous streamwise velocity from a DNS of a ZPG TBL flow at $Re_\theta \approx 2,500$ (Schlatter and Örlü 2010). Filled contours indicate 10, 30, 50, 70, and 90 % of the local peak PDF value (marked

as a dashed white line), whereas the black dashed lines include all sampled velocity signals, i.e. the extreme values of the PDF. Note that the appearance of bulges within the viscous sublayer is an artifact due to the sparse number of wall-normal positions, i.e. $y^+ = 1.69, 2.80,$ and 4.97

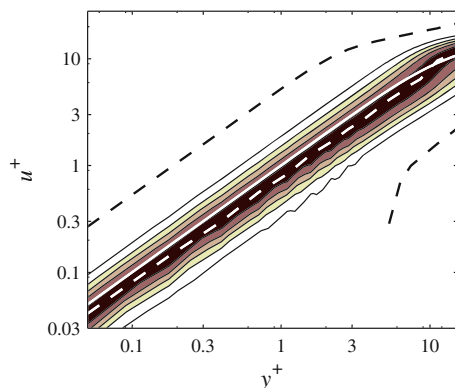


Fig. 2 Reproduction of Fig. 1b for a channel flow DNS at $h^+ = 590$ with a finer resolved wall-normal spacing, i.e. with ten wall-normal positions within the viscous sublayer, both to avoid the artificial bulges seen in Fig. 1b and to demonstrate the self-similarity of the PDFs within the viscous sublayer

An advantageous feature of the CDF is that its limiting values both at low and high u are known (0 and 1, respectively) and that there is no scaling associated with these values. This also indicates that if one has a problem with, for instance, the instantaneous low velocities of a turbulent signal (e.g. due to calibration errors), it will not affect F in the high velocity range.

By using DNS data from turbulent boundary layer or channel flow simulations, it can be shown that for $y^+ < 5$, the PDFs are very close to self-similar as discussed above. The same is true for F which is plotted in Fig. 3 for a number of different wall-normal positions for the same data as in Fig. 2. Here, the horizontal axis is normalized with the distance from the wall which takes into account that the mean values increase according to the linear velocity profile and would make all CDFs collapse if they were truly self-similar, which is actually what is observed

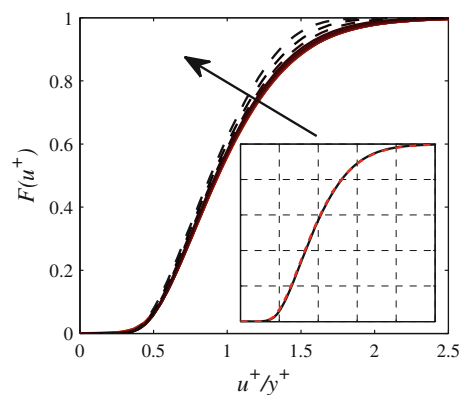


Fig. 3 The CDF near the wall obtained from channel flow DNS data at $h^+ = 590$. Plotted are 13 profiles in total from $y^+ = 0.04$ to 7.4 , whereas the 10 profiles closest to the wall (up to $y^+ = 4.4$) are given through solid lines, and the profiles at $y^+ = 5.3, 6.3,$ and 7.4 are indicated through dashed ones. Direction of arrow indicates increasing y^+ . The insert compares the CDF for $y^+ = 2.8$ with results from DNS from a ZPG TBL flow at $Re_\theta \approx 2,500$, corresponding to $Re_\tau \approx 830$, (dashed line)

for the positions within the viscous sublayer. To ensure that the observed self-similarity for $y^+ < 5$ for channel flows is equivalent to the one of the ZPG TBLs, the CDF of the boundary-layer data (shown in Fig. 1) are presented in the insert and are compared to the channel flow data at $y^+ = 2.8$.

3.4 Lognormal velocity fluctuations

As apparent from Figs. 1 and 2, the PDF contour lines within the viscous sublayer do not only become parallel to each other, when the velocity space is plotted logarithmically, but also appear equidistantly spaced. This is a clear indication for a lognormal behavior, and this idea will be

Table 1 Moments of the fluctuating wall shear stress from DNS of a ZPG TBL flow (Schlatter and Örlü 2010), parameters of the lognormal PDFs fitted to the DNS results, higher-order moments extracted from integration of the lognormal distribution or

equivalently through evaluation of algebraic relations given in Eqs. 5–8, as well as through integration over a truncated ($\tau_w^+ \in [0, 3]$) lognormal PDF

	DNS				Eq. 3		logn PDF or Eqs. 5–8				Truncated logn PDF			
	Mean	Std/mean	Skew	Flat	μ	σ	Mean	Std/mean	Skew	Flat	Mean	Std/mean	Skew	Flat
1,100	1.00	0.411	0.97	4.70	−0.063	0.417	1.02	0.44	1.40	5.31	1.02	0.42	1.11	4.56
2,500	1.00	0.420	1.03	5.01	−0.067	0.421	1.02	0.44	1.41	5.40	1.01	0.43	1.12	4.56
4,000	1.00	0.426	1.07	5.19	−0.069	0.425	1.02	0.45	1.42	5.47	1.01	0.43	1.12	4.56

Note that (a) the number of decimal points for the results from the lognormal PDF is not to be considered the accuracy of the fit nor its extracted values, but serves here merely to indicate the weak Reynolds number trend, and (b) the fitting constants and the obtained moments differ slightly when fitting the lognormal CDFs to the DNS results

exploited by considering the PDF and CDF of a lognormal distribution (Landahl and Mollo-Christensen 1992)

$$f(u, \mu, \sigma) = \frac{1}{\sqrt{2\pi\sigma u}} \exp\left[-\frac{1}{2\sigma^2}(\ln(u) - \mu)^2\right] \quad (3)$$

$$F(u, \mu, \sigma) = \frac{1}{2} \operatorname{erfc}\left[-\frac{\ln(u) - \mu}{\sqrt{2}\sigma}\right]. \quad (4)$$

By fitting relation Eqs. 3 or 4 to the PDF or CDF from DNS data, the constants μ and σ are obtained, and the analytical relations in Eqs. 3 and 4 are found to represent the PDF and CDF of the DNS data to a high degree. These distributions depend on only two parameters, i.e. μ is close to (but not exactly) zero, and σ is related to the local rms value as apparent from Table 1 and shown in the following. Consequently, the knowledge of the rms of the fluctuating wall shear stress describes the PDF and CDF, and in turn, the (higher order) moments can easily be extracted either through algebraic relations²,

$$\operatorname{mean}(\mu, \sigma) = \exp[\mu + \sigma^2/2] \quad (5)$$

$$\operatorname{var}(\mu, \sigma) = (\exp[\sigma^2] - 1) \exp[2\mu + \sigma^2] \quad (6)$$

$$\operatorname{skew}(\sigma) = (\exp[\sigma^2] + 2) \sqrt{\exp[\sigma^2] - 1} \quad (7)$$

$$\operatorname{flat}(\sigma) = \exp[4\sigma^2] + 2 \exp[3\sigma^2] + 3 \exp[2\sigma^2] - 3, \quad (8)$$

or by integration of the PDF.

Utilization of the algebraic relations Eqs. 5–8 yields limiting values for the mean and variance as well as the skewness and flatness factor, which are reasonable close to DNS results, however, due to the one-sided unboundedness, i.e. $u \in [0, +\infty]$ of the lognormal distribution the obtained lognormal distribution is more positively skewed and more peaked. The integration over a truncated lognormal PDF instead resembles the DNS results even better. This has exemplarily been demonstrated in Table 1, where μ and σ have been obtained by fitting Eq. 3 to the

PDF of the wall shear stress fluctuations from a ZPG TBL flow at $Re_\theta = 1,100, 2,500,$ and $4,000$ (cf. next Section and Fig. 4), and the corresponding first four moments from the DNS, the aforementioned algebraic relations for the lognormal distribution as well as the integration over a truncated lognormal PDF are given.

Although lognormal distributions have been found to describe various phenomena in wall turbulence, e.g. spanwise streak spacing, time intervall between burst events (Smith and Metzler 1983; Klewicki et al. 1995; Rao et al. 1971), they have—to the authors’ knowledge—not been associated with the streamwise velocity or wall shear stress fluctuations within the viscous sublayer. The finding that the distributions are in fact very close to lognormal and are well described by two physics-based constants is of particular importance from a measurement technique point of view. In particular, it is common practice to compare (or validate) innovative methods, as e.g. the laser gradient

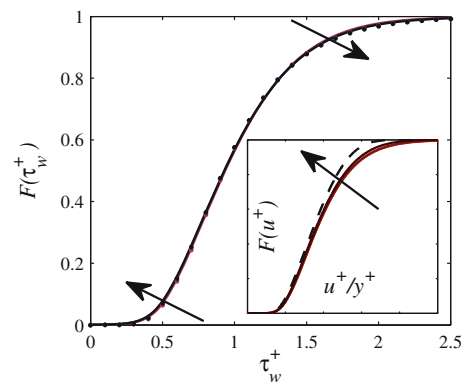


Fig. 4 The CDF of the wall shear stress fluctuations from a ZPG TBL DNS for $Re_\theta \approx 1,100, 2,500,$ and $4,000$ (Schlatter and Örlü 2010). Dots indicate the CDF distribution based on Eq. 4 for the three different Reynolds numbers with the constants given in Table 1. Arrows show the direction of increasing Re_θ , although the differences are hardly notable. Insert shows CDF for ZPG TBL data near the wall at $Re_\theta \approx 2,500$ for $y^+ = 1.69, 2.80, 4.97,$ and 7.77 . First three profiles are indicated through solid and the last through a dashed line. Note that the first two profiles are overlapping throughout the whole velocity space. Arrow shows the direction of increasing y^+

² Equivalently, the lognormal distribution parameters, μ and σ , can be obtained through the mean and variance of the PDF, viz. $\mu = \ln(\operatorname{mean}^2 / \sqrt{\operatorname{var} + \operatorname{mean}^2})$ and $\sigma = \sqrt{\ln(\operatorname{var} / \operatorname{mean}^2 + 1)}$.

meter (Naqwi and Reynolds 1991; Obi et al. 1996), the micro-shear stress imager (Miyagi et al. 2000), or the micro-pillar shear stress sensor (Brücker et al. 2005; Große and Schröder 2009) by means of their measured PDF of the wall shear stress fluctuations.

At this point, a note of caution might be appropriate, since “the lognormal distribution is [...] an approximation, often quite close to observations, but still possibly wrong by a large factor for values far from the mean” (Landahl and Mollo-Christensen 1992). Nevertheless, the lognormal distribution, with the mean and standard deviation (std) as its describing parameters, is a simple but sufficiently accurate description for the purpose of the present paper. In this respect, the accuracy of the lognormal distribution to describe the streamwise velocity fluctuations within the viscous sublayer is comparable to that of the general distribution functions (with seven parameters) or the hyperbolic distributions (with four parameters) described by Barndorff-Nielsen (1979). For the case that a distribution function is sought to describe the entire boundary layer, rather than the viscous sublayer only, in particular, the hyperbolic distribution functions have been found to be capable of this (Durst et al. 1987).

3.5 A note on Reynolds number effects

As shown above, the PDFs and CDFs can accurately be described by a lognormal distribution and the rms of the wall shear stress fluctuations, or the limiting local rms value in the case of streamwise velocity signals within the viscous sublayer is directly related to the governing parameter describing the distribution function. Since the study by Alfredsson et al. (1988), a value of 0.40 has widely been accepted for channel and pipe as well as ZPG TBL flows and only recently, mainly due to the emergence

of DNS results spanning a decade in Reynolds number, has a weak Reynolds number effect been shown to exist (Fischer et al. 2001; Abe et al. 2004; Buschmann et al. 2009). Despite the found weak increase with Reynolds number, e.g.

$$\tau_{w,rms}^+ = 0.298 + 0.017 \ln Re_\tau$$

for ZPG TBL flows (Schlatter and Örlü 2010), also documented in the DNS results in Table 1, the effect on the PDF or CDF is barely visible, as illustrated in Fig. 4, where the CDF of the wall shear stress fluctuations is shown. The documented results from the integration over a truncated PDF also confirm that the inherent Reynolds number trend is barely noticeable. The figure also indicates, based on the results from relation Eq. 4 for the Reynolds numbers at $Re_\theta = 1,100, 2,500, \text{ and } 4,000$, that the lognormal distribution provides an accurate description of the CDFs.

4 Exploiting the self-similarity of the PDF ...

Having now established the self-similarity of the distribution function of the streamwise velocity fluctuations within the viscous sublayer, we now describe how this information can be exploited to determine both the wall location and the friction velocity.

4.1 ... to determine the wall location

Now, consider the PDF of the streamwise velocity component from a ZPG TBL flow in Fig. 5 measured with hot-wire anemometry at around the same Reynolds number as the previously shown DNS. Already in the standard plot, depicted in Fig. 5a, it is clear that close to the wall there are some problems by heat conduction effects especially in the

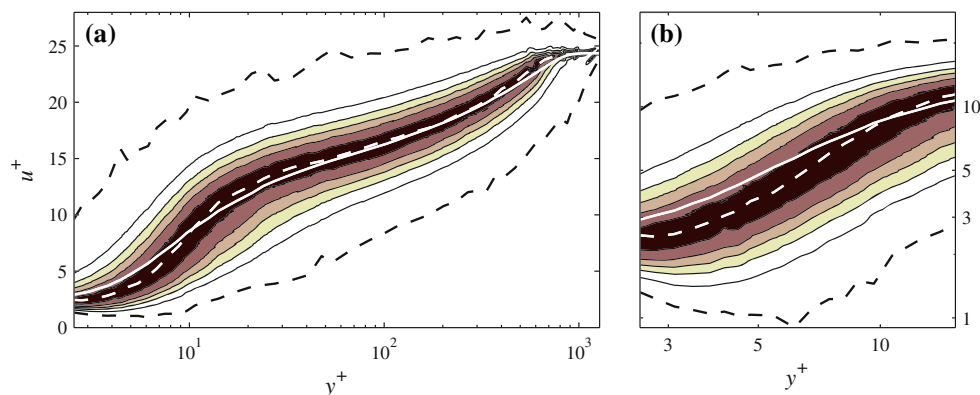


Fig. 5 Mean streamwise velocity over wall-normal position scaled in inner variables, U^+ versus y^+ , (white line) plotted above the PDF of the instantaneous streamwise velocity from hot-wire measurements in a ZPG TBL flow at $Re_\theta \approx 2,500$ (Örlü 2009). Filled contours indicate 10, 30, 50, 70, and 90 % of the local peak PDF value (marked

as a dashed white line), whereas the black dashed lines include all sampled velocity signals, i.e. the extreme values of the PDF. Note the similarity of this graph to the equivalent representation of the DNS results in Fig. 1

low-velocity part of the PDF. In Fig. 5b, the near-wall region is expanded, and it clearly demonstrates that the low velocities of the PDF are affected up to around $y^+ \approx 7-8$, while the contour lines pertaining to higher velocity PDF levels seem to be unaffected. Recently, the so-called diagnostic plot has been proposed by Alfredsson and Örlü (2010) to determine where wall interference affects the readings of both the mean velocity and rms. This plot has been illustrated in Fig. 6, where the same data as those in Fig. 5 have been used. It seems that measurements of both the mean and rms of the streamwise velocity below $y^+ \approx 4$ are significantly affected by wall interference effects (while its mean value still follows the linear velocity profile down to $y^+ \approx 3$).

For hot-wire measurements of F obtained for various positions in the wall region, it is clear that the turbulent signal is mainly affected by heat transfer to the wall during periods of low streamwise velocity and not necessarily for periods of high velocity. This can for instance be evinced from Fig. 7, where the CDFs from near-wall hot-wire measurements are depicted. While the closest near-wall profiles are affected throughout the velocity space, i.e. $0 \leq F(u^+) \leq 1$, the remaining profiles within $3.8 \leq y^+ \leq 4.8$ collapse on each other. Also the profiles above the viscous sublayer do not adhere to the self-similar scaling, the lower-velocity part of the CDF, i.e. $F(u^+) < 0.6$, collapses on the self-similar viscous sublayer scaling beyond 7 wall units. This makes it possible to use only the velocity data where F is unaffected by heat transfer, i.e. where the velocity corresponding to a given value of F varies linearly with the wall distance. This means that by plotting the u -value versus the y -position for a given F should result in a straight line that should go through the origin of the yu -plane. By

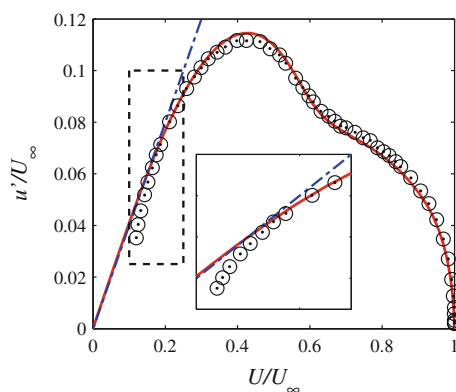


Fig. 6 Diagnostic plot for the data in Fig. 5. It is seen close to the wall that the data points deviate from the linear profile (here, with a slope of 0.4 indicated through the dash-dotted line), and this is mainly due to heat conduction to the wall. Such an effect results in both too high mean velocity and too low rms. Solid line is from the DNS at the same Re_θ

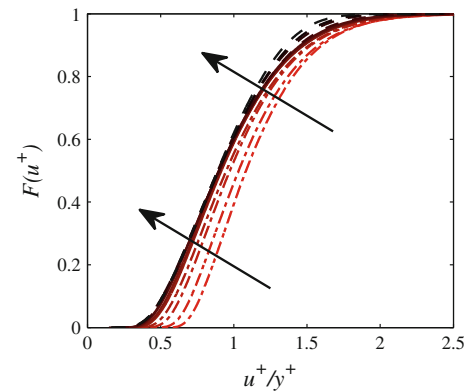


Fig. 7 The CDF for measurements near the wall. Experimental data from Örlü (2009) at $y^+ = 2.5, 2.8, 3.1, 3.4, 3.8, 4.1, 4.6, 4.8, 5.4, 6.1, 6.8, 7.5$. First, four profiles are effected through heat conduction (dash-dotted), while the last four profiles (dashed) start to deviate from the self-similar distribution above $F(u^+) > 0.6$. Arrows show the direction of increasing y^+

doing so for a number of values of F , a good estimate of the wall position is possible to obtain.

In order to illustrate the proposed idea, Fig. 8a depicts four CDF contours obtained from boundary-layer DNS together with a linear fit through the three available near-wall points within the viscous sublayer. Although only four contour lines have been depicted here for clarity, more can and should be employed, due to the few suitable wall-normal positions that can be used, in order to obtain a statistically converged estimate of the wall position. True self-similarity would lead the contour lines to be parallel in a log-log plot and intersecting with each other at the wall in linear-linear plot, which is what actually is observed in Fig. 8a,b. In Fig. 9a,b, the experimental data are plotted, and it is clearly seen how the higher values of the CDF give a good estimate of the wall position, but that also lower values can be used as long as they are not too close to the wall. This means that both the velocity by itself but also the distance to the wall are important when determining when wall interference effects come into play.

As evident from Figs. 8a and 9a, displaying the CDF contour lines in a log-log plot exposes the deviation from the self-similar behavior and thereby marks the upper limit for the data to be employed. From the employed DNS, this can clearly be related to $y^+ > 5$. Although this region, i.e. the points for which $y^+ > 5$, is not known *a priori* in an experiment, it can be interfered by considering the region in which the data deviate from a parallel line pattern. Due to the additional heat losses to the wall, there is a need to define a lower limit when using hot wires. This lower limit can similarly be defined through its deviation from the parallel line pattern, as evident from Fig. 9a.

The demarcation lines used in Fig. 9 were constructed by utilizing the diagnostic plot to identify an appropriate

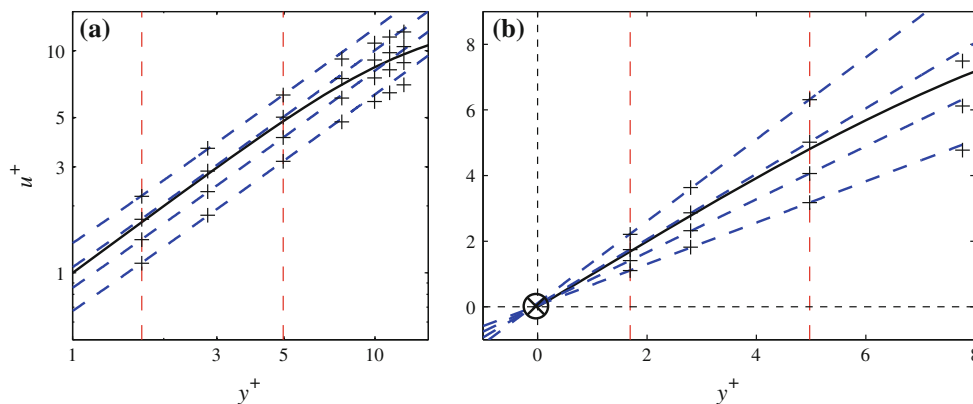


Fig. 8 Proof of concept for the employment of the self-similarity of the CDFs in the viscous sublayer to extract the wall position by means of DNS data (Schlatter and Örlü 2010). $F(u^+) = 0.2, 0.4, 0.6$, and 0.8 has been used. Linear fits through the closest three near-wall points (+) are indicated through *dashed lines*. *Solid line* indicates the mean

streamwise velocity component and \otimes the extracted wall position. For the data shown here, as well as other tests at different Reynolds numbers or with different heights of contour levels, the extracted wall position was well within $\pm 0.05\ell_*$

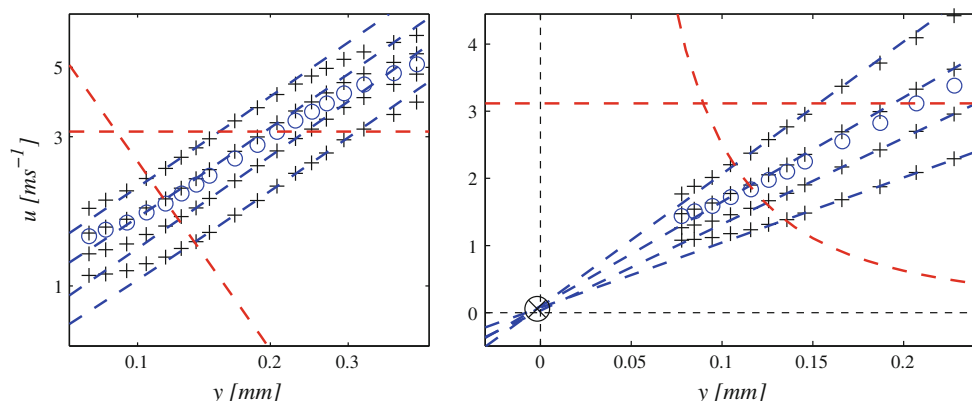


Fig. 9 Application of concept for the employment of the self-similarity of the CDFs in the viscous sublayer to extract the wall position by means of hot-wire data Experimental data from (Örlü 2009). Levels and *symbols* as in Fig. 8 and *circles* are the mean streamwise velocity component from the experimental data. *Dashed line* with -2 -slope indicates the lower limit of near-wall points free

from heat transfer to the wall detected through the diagnostic plot, whereas the *vertical dashed lines* indicate the upper limit in which the linear fit was applied to the CDF contour levels. For the data shown here, u_τ and ℓ_* are 0.49 ms^{-1} and 0.03 mm , respectively

measurement point from where on the data cannot be trusted anymore and draw an empirical -2 -slope through the employed CDF contour line corresponding to the lowest velocity fluctuation. The slope is based on mean velocity results from early investigations on wall proximity effects on hot-wire readings within the viscous sublayer (Oka and Kostic 1972; Hebbar 1980; Bhatia et al. 1982), which indicate such a scaling for approximately $1.5 < y^+ < 6$ (see e.g. Bhatia et al. 1982, Fig. 13). As apparent from Fig. 9a, this seems to agree fairly well with the CDF contour lines when considering the demarcation line for the deviation from the parallel line pattern. Note, however, that such a demarcation line is not necessary, since the disregarded region can be also be inferred by mere observation, through the deviation from the parallel line pattern.

4.2 ... to determine the friction velocity

To obtain a value of the friction velocity is slightly more intricate. Here, we use the information from the DNS, Figs. 3 and 4, and the assumption that the CDF is self-similar within the viscous sublayer and even up to about $y^+ = 7$ when only considering the lower part of the CDF ($F < 0.6$). By now iterating the value of u_τ until the CDF overlaps with the CDF of the simulation for values of y^+ in the approximate range 4–7 where also the low-velocity part should not be affected by the heat conduction. If this is done for some different y -values, a good estimate of u_τ can be established. Figure 10 demonstrates the sensitivity of the CDF variations in terms of friction velocity and clearly demonstrates that the CDF is quite sensitive to a change in

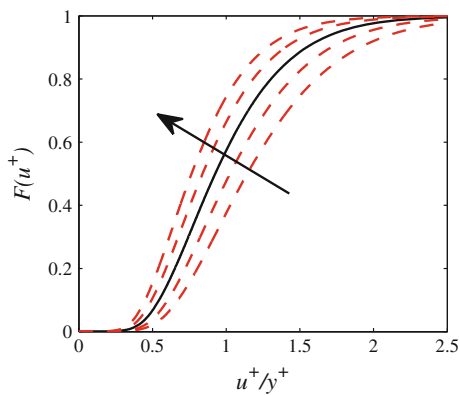


Fig. 10 Application of concept for the employment of the self-similarity of the CDFs in the viscous sublayer to obtain the friction velocity. Dashed lines indicate ± 5 and 10% tolerances in u_τ , with the arrow pointing toward increasing u_τ values

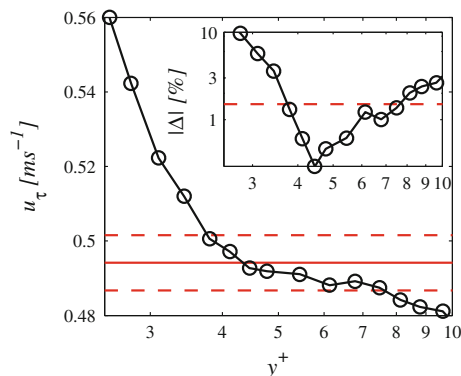


Fig. 11 Application of concept for the employment of the self-similarity of the CDFs in the viscous sublayer to obtain the friction velocity demonstrated on the experimental ZPG TBL data depicted in Fig. 7. The CDFs have been fitted to the lognormal distribution, i.e. Eq. 4, by considering data in the range $0.05 < F < 0.6$. Horizontal solid and dashed lines indicate the u_τ value obtained from oil-film interferometry and $\pm 1.5\%$ tolerance limits, respectively. Insert depicts the relative error to the value obtained through oil-film interferometry

u_τ , viz. $\sim u_\tau^{-2}$, while the changes observed for variations in y^+ or Reynolds number effects are less significant as evident from Figs. 3 and 4.

The proposed method is now applied by utilizing the CDFs obtained from a ZPG TBL experiment, shown in Fig. 7. The CDFs have been fitted to the lognormal distribution by considering only data in the range $0.05 < F < 0.6$. Hereby, it was found that $(\mu, \sigma) = (-0.08, 0.42)$ gives a sufficiently accurate fit for all employed DNS data for the purpose of the present paper for both channel and ZPG TBL flows at the wall and throughout the viscous sublayer when considering Eq. 4. The obtained results from the proposed method have been compared to the value of the friction velocity obtained by means of oil-film interferometry and are shown in Fig. 11.

Note, however, the used reference value has an inherent uncertainty of up to $\pm 1.5\%$ (Pailhas et al. 2009) and serves therefore merely for a comparison. It is interesting to point out that the obtained u_τ value lies within the mentioned tolerances, as long as the measurement points clearly affected by additional heat losses are neglected, viz. the first 4 near-wall points (dash-dotted lines in Fig. 4). It is also shown that the CDFs outside the viscous sublayer can be employed and still give an accurate estimate of the friction velocity, due to the fact that the CDF for the lower velocities, i.e. $F < 0.6$, remains self-similar up to around $y^+ = 7$.

5 Conclusion

This paper shows, based on results from DNS in channel and ZPG TBL flows, that the PDFs and CDFs of the streamwise velocity are self-similar within the viscous sublayer and retain a certain degree of self-similarity up to about $y^+ = 7$ at least for the lower half of the CDFs. Furthermore, it has been shown that the PDFs and CDFs can be described by means of a lognormal distribution, where the describing constants are directly related to the mean and rms of the fluctuating wall shear stress. It is shown that this fact can be exploited to obtain accurate estimates of the wall position by using only parts of the CDF that are self-similar and not affected by heat transfer to the wall. After determining the wall position, one can use the CDF to obtain an estimate of the friction velocity. Both proposed methods have been tested against DNS data and applied on hot-wire measurements in a ZPG TBL flow. Extensive tests on experimental datasets indicate that the wall position can be determined with an accuracy of $\pm 0.1\ell_*$, while the friction velocity could be estimated to within an accuracy, which is associated with oil-film interferometry, i.e. $\pm 1.5\%$ (Pailhas et al. 2009). Whether it is possible to extend this method to flows with pressure gradients is an open question and will be investigated in the future.

Acknowledgements Financial support from the Swedish Research Foundation (VR) is gratefully acknowledged. Computer time was provided by SNIC (Swedish National Infrastructure for Computing) with a generous grant by the Knut and Alice Wallenberg (KAW) Foundation.

References

- Abe H, Kawamura H, Choi H (2004) Very large-scale structures and their effects on the wall shear-stress fluctuations in a turbulent channel flow up to $Re_\tau = 640$. *J Fluid Eng* 126:835–846
- Alfredsson PH, Johansson AV, Haritonidis J, Eckelmann H (1988) The fluctuating wall-shear stress and the velocity field in the viscous sublayer. *Phys Fluids* 31:1026–1033

- Alfredsson PH, Örlü R (2010) The diagnostic plot—a litmus test for wall bounded turbulence data. *Eur J Mech B-Fluid* 29:403–406
- Barndorff-Nielsen O (1979) Models for non-Gaussian variation, with applications to turbulence. *Proc R Soc London Ser A* 368:501–520
- Bhatia J, Durst F, Jovanovic J (1982) Corrections of hot-wire anemometer measurements near walls. *J Fluid Mech* 123:411–431
- Brücker C, Spatz J, Schröder W (2005) Feasibility study of wall shear stress imaging using microstructured surfaces with flexible micropillars. *Exp Fluids* 39:464–474
- Buschmann MH, Gad-el-Hak M (2010) Kolmogorov scaling of turbulent flow in the vicinity of the wall. *Phys D Nonlinear Phenom* 239:1288–1295
- Buschmann MH, Indinger T, Gad-el-Hak M (2009) Near-wall behavior of turbulent wall-bounded flows. *Int J Heat Fluid Flow* 30:993–1006
- Chevalier M, Schlatter P, Lundbladh A, Henningson DS (2007) SIMSON—a pseudo-spectral solver for incompressible boundary-layer flow. *Tech Rep TRITA-MEK 2007:07*, Royal Institute of Technology, Stockholm, Sweden
- Chew Y, Shi S, Khoo BC (1995) On the numerical near-wall corrections of single hot-wire measurements. *Int J Heat Fluid Flow* 16:471–476
- Durst F, Jovanovic J, Kanevce L et al (1987) Probability density distribution in turbulent wall boundary-layer flows. In: Durst F (eds) *Turbulent shear flows 5*. Springer, Berlin, pp 197–220
- Durst F, Kikura H, Lekakis I, Jovanovic J, Ye Q (1996) Wall shear stress determination from near-wall mean velocity data in turbulent pipe and channel flows. *Exp Fluids* 20:417–428
- Durst F, Zanoun ES (2002) Experimental investigation of near-wall effects on hot-wire measurements. *Exp Fluids* 33:210–218
- Durst F, Zanoun ES, Pashtrapanska M (2001) In situ calibration of hot wires close to highly heat-conducting walls. *Exp Fluids* 31:103–110
- Eckelmann H (1974) The structure of the viscous sublayer and the adjacent wall region in a turbulent channel flow. *J Fluid Mech* 65:439–459
- Fischer M, Jovanovic J, Durst F (2001) Reynolds number effects in the near-wall region of turbulent channel flows. *Phys Fluids* 13:1755–1767
- Große S, Schröder W (2009) High Reynolds number turbulent wind tunnel boundary layer wall-shear stress sensor. *J Turbulence* 10:1–12
- Hebbar K (1980) Wall proximity corrections for hot-wire readings in turbulent flows. *DISA Inf* 25:15–16
- Hultmark M, Bailey SCC, Smits AJ (2010) Scaling of near-wall turbulence in pipe flow. *J Fluid Mech* 649:103–113
- Khoo BC, Chew Y, Li G (1997) Effects of imperfect spatial resolution on turbulence measurements in the very near-wall viscous sublayer region. *Exp Fluids* 22:327–335
- Klewicki JC, Metzger M, Kelner E, Thurlow E (1995) Viscous sublayer flow visualizations at $Re_\theta \cong 1500000$. *Phys Fluids* 7:867–863
- Landahl M, Mollo-Christensen E (1992) *Turbulence and random processes in fluid mechanics*, 2nd ed. Cambridge University Press, Cambridge
- Lindgren B, Johansson AV, Tsuji Y (2004) Universality of probability density distributions in the overlap region in high Reynolds number turbulent boundary layers. *Phys Fluids* 16:2587–2591
- Marusic I, Heuer WDC (2007) Reynolds number invariance of the structure inclination angle in wall turbulence. *Phys Rev Lett* 99:114504
- Miyagi N, Kimura M, Shoji H, Saima A, Ho CM, Tung S, Tai YC (2000) Statistical analysis on wall shear stress of turbulent boundary layer in a channel flow using micro-shear stress imager. *Int J Heat Fluid Flow* 21:576–581
- Monin AS, Yaglom AM (1971) *Statistical fluid mechanics: mechanics of turbulence*. vol. I. MIT Press, Cambridge
- Morrison JF, McKeon B, Jiang W, Smits AJ (2004) Scaling of the streamwise velocity component in turbulent pipe flow. *J Fluid Mech* 508:99–131
- Moser RD, Kim J, Mansour N (1999) Direct numerical simulation of turbulent channel flow up to $Re_\tau = 590$. *Phys Fluids* 11:943–945
- Naqwi A, Reynolds W (1991) Measurement of turbulent wall velocity gradients using cylindrical waves of laser light. *Exp Fluids* 10:257–266
- Obi S, Inoue K, Furukawa T, Masuda S (1996) Experimental study on the statistics of wall shear stress in turbulent channel flows. *Int J Heat Fluid Flow* 17:187–192
- Oka S, Kostic Z (1972) Influence of wall proximity on hot-wire velocity measurements. *DISA Inf* 13:29–33
- Örlü R (2009) *Experimental studies in jet flows and zero pressure-gradient turbulent boundary layers*. PhD thesis, Royal Institute of Technology, Stockholm, Sweden
- Örlü R, Fransson JHM, Alfredsson PH (2010) On near wall measurements of wall bounded flows—the necessity of an accurate determination of the wall position. *Prog Aero Sci* 46:353–387
- Örlü R, Schlatter P (2011) On the fluctuating wall shear stress in zero pressure-gradient turbulent boundary layer flows. *Phys Fluids* (in press)
- Pailhas G, Barricau P, Touvet Y, Perret L (2009) Friction measurement in zero and adverse pressure-gradient boundary layer using oil droplet interferometric method. *Exp Fluids* 47:195–207
- Rao K, Narasimha R, Narayanan M (1971) The ‘bursting’ phenomenon in a turbulent boundary layer. *J Fluid Mech* 48:339–352
- Rüedi J-D, Duncan R, Imayama S, Chauhan K (2009) Accurate and independent measurements of wall-shear stress in turbulent flows. *Bull Am Phys Soc* 54:20
- Schlatter P, Örlü R (2010) Assessment of direct numerical simulation data of turbulent boundary layers. *J Fluid Mech* 659:116–126
- Schlatter P, Örlü R, Li Q, Brethouwer G, Fransson JHM, Johansson AV, Alfredsson PH, Henningson DS (2009) Turbulent boundary layers up to $Re_\theta = 2500$ studied through simulation and experiment. *Phys Fluids* 21:051702
- Smith C, Metzler S (1983) The characteristics of low-speed streaks in the near-wall region of a turbulent boundary layer. *J Fluid Mech* 129:27–54
- Tsuji Y, Nakamura I (1999) Probability density function in the log-law region of low Reynolds number turbulent boundary layer. *Phys Fluids* 11:647–658
- Wenzhong L, Khoo BC, Diao X (2006) The thermal characteristics of a hot wire in a near-wall flow. *Int J Heat Mass Transfer* 49:905–918
- Wu X, Moin P (2006) A direct numerical simulation study on the mean velocity characteristics in turbulent pipe flow. *J Fluid Mech* 608:81–112